Title: Mosquito lipids regulate *Plasmodium* sporogony and infectivity to the mammalian host

Giulia Costa[1], Maarten Eldering[1,2], Randall L. Lindquist[3], Anja E. Hauser[3,4], Robert Sauerwein[2], Christian Goosmann[1], Volker Brinkmann[1] and Elena A. Levashina[1]*

Affiliations:

[1] Max Planck Institute for Infection Biology, Berlin, Germany

[2] Radboud University Medical Center, Nijmegen, The Netherlands

[3] German Rheumatism Research Centre (DRFZ), Berlin, Germany

[4] Charité-Universitätsmedizin Berlin, Germany

* Corresponding author: levashina@mpiib-berlin.mpg.de

Summary

Malaria is a human parasitic disease that is transmitted by a mosquito vector. *Plasmodium* parasites, the causative agents, differ in their infectivity and virulence to the mammalian host, but the mechanistic underpinnings of this variation remain unknown. As mosquitoes provide a nutrient-rich niche for development of transmissible stages, we examined the role of lipids in parasite development and infectivity by disrupting lipid trafficking in mosquito adults. We show that depleting the major mosquito lipoprotein lipophorin deprives parasites of neutral lipids, arrests oocysts growth and impairs sporozoite formation. Importantly, lipid deficiency decreases parasite mitochondrial membrane potential and severely compromises sporozoite infectivity and virulence in the mammalian host. Our findings demonstrate the requirement of mosquito lipids for *Plasmodium* metabolism, and uncover the mitochondrial contribution to parasite infectivity and virulence. By drawing a connection between vector nutrition and malaria virulence, our results redefine the paradigm of vector-host-pathogen interactions.

INTRODUCTION

Nutrition plays a key role in host-pathogen interactions, as parasites hijack host metabolites to survive and propagate. *Plasmodium* parasites, the causative agents of malaria, are no exception. Malaria is the deadliest infectious disease transmitted to humans by anopheline mosquitoes. Multiple reports have implicated larval diet and adult blood meals in determining parasite loads within a mosquito (Moller-Jacobs et al., 2014; Okech et al., 2004; Ponnudurai et al., 1989; Shapiro et al., 2016; Takken et al., 2013; Vantaux et al., 2016). Indeed, females produced by undernourished larvae are poor *Plasmodium* hosts (Moller-Jacobs et al., 2014; Shapiro et al., 2016; Takken et al., 2013; Vantaux et al., 2016), although additional blood feedings improve parasite survival (Okech et al., 2004; Ponnudurai et al., 1989). Together with proteins and carbohydrates, lipids constitute important building blocks of nutrition since they provide living organisms with energy, serve as the structural materials of cell and organelle membranes, and function as signaling molecules. In contrast to the defined role of lipids in *Plasmodium* development within a mammalian host (Grellier et al., 1991; Itoe et al., 2014; Lauer et al., 2000), the contributions of mosquito lipids remain unknown. Mosquitoes acquire lipids from their diet and store them in the fat body, an insect equivalent of mammalian liver. Lipid levels in the tissues are maintained by lipophorin (Lp), the hemolymph-circulating transporter that shuffles hydrophobic lipids between the fat body and energy demanding tissues (Atella et al., 2006; Van der Horst et al., 2009). The blood meal brings to the mosquito massive lipid resources that, in the course of the first days, are routed by Lp from the midgut to the developing ovaries for egg development and to the fat body for storage. Disrupting Lp function aborts ovary development and renders the parasites more vulnerable to the mosquito complement-like system (Mendes et al., 2008; Rono et al., 2010). Here we exploited Lp deficiency to examine the role of mosquito lipids in *Plasmodium* sporogonic development, transmission and virulence to the mammalian host.

RESULTS

49 **Disruption of lipid trafficking between mosquito tissues mitigates *Plasmodium***
50 **sporogony**

51 We first investigated whether Lp depletion disrupts lipid trafficking between mosquito
52 tissues. To this end, females were injected with *dsRNA* against Lp and then fed on
53 *Plasmodium*-infected blood. Lipid content of the tissues was gauged by Nile Red staining
54 (Rudolf and Curcio, 2009). In control mosquitoes, blood feeding significantly increased
55 levels of the Nile Red signal in the midgut and in the ovaries, but no change was
56 observed in the fat body (Figure 1, A and B). While Lp depletion transiently increased
57 lipid levels in the midgut, it abrogated the feeding-induced increase in lipid levels in the
58 ovaries (Figure 1, A and B). Again, no changes in lipid levels were detected in the fat
59 body. We conclude that blocking the blood meal-induced lipid trafficking by Lp
60 depletion efficiently disrupts lipid transport between mosquito tissues.

61 We next examined the effects of disruption of lipid trafficking on *Plasmodium*
62 development. To prevent large losses at early stages of parasite development inflicted by
63 the mosquito complement-like system in the absence of Lp (Mendes et al., 2008; Rono et
64 al., 2010), all infection experiments were performed with immune-deficient mosquitoes
65 (Pompon and Levashina, 2015). When mosquitoes were infected with *P. falciparum*, a
66 significant decrease in the size of mature oocysts was observed in Lp-depleted
67 mosquitoes (Figure 1C). Strikingly, inhibition of lipid trafficking led to a 5-fold decrease
68 in the number of salivary gland sporozoites (Figure 1D). Similar effects on sporogony
69 and sporozoite loads were observed for *P. berghei* (Figure 1C and D). Further, the
70 comparable decrease in numbers of midgut and salivary gland sporozoites suggested that
71 Lp depletion inhibited parasite sporogony in the oocysts (Table S1). Taken together,
72 these results show that Lp-mediated lipid trafficking is essential for sporogony of human
73 and rodent *Plasmodium* parasites.

74

75 **Lp-transported lipids are essential for *Plasmodium* sporogonic development**

76 To investigate how disruption of lipid trafficking affected parasite sporogony, we
77 followed development of *P. berghei* GFP-expressing oocysts by fluorescence microscopy

(Franke-Fayard et al., 2004). A significant decrease in oocyst size was observed in Lp-deficient mosquitoes 7 days post infection (dpi) (Figure 2A), indicating that Lp deficiency arrests parasite growth at the onset of sporogony. We next examined whether oocysts accumulated lipids and the role of Lp in this process. A clear Nile Red signal was observed in the peripheral cytoplasm and vesicles (Figure 2B). Importantly, this signal was absent in the oocysts of Lp-depleted mosquitoes (Figure 2B and Figure S1A), suggesting that Lp is required for parasite provision with mosquito lipids. To investigate whether Lp was taken up by oocysts together with its lipid cargo, we used antibodies directed against the protein moiety of the Lp particle (Rono et al., 2010). In controls, The number of Lp-positive oocysts increased over time (25% and 72% at 7 and 13 dpi, respectively, Figure 2A). Lp signal was observed on the surface but not inside the oocysts (Figure 2C). As expected, no signal was detected in Lp-depleted mosquitoes (Figure 2C). Progressive accumulation of Lp on the parasite surface suggests that *Plasmodium* exploits Lp particles for lipid delivery to the oocysts rather than for uptake. Transmission electron microscopy analysis further confirmed that Lp depletion did not impact development of young oocysts (7 dpi) which displayed normal ultrastructure (Figure 2D and E). Instead, in Lp-depleted mosquitoes, almost half of the mature oocysts displayed cytoplasmic vacuolization and lack of classical membrane retractions characteristic of initiation of sporulation (Figure 2F). Moreover, these aberrant oocysts were surrounded by the electron-dense actin zones associated with dead ookinetes (Shiao et al., 2006) (Figure 2E and Figure S2). Collectively, these observations indicate that lipid restriction inhibits oocyst sporulation and induces the death of mature oocysts. Therefore, mosquito lipids represent a limiting step in parasite development in the midgut.

Mosquito lipids control *Plasmodium* virulence to the next mammalian host

As some sporozoites were able to complete their development in spite of massive oocyst die-off (Figure 1D), we examined the effect of lipid starvation on *Plasmodium* transmission. In these experiments, naïve mice were exposed to the bites of *P. berghei*-infected control or Lp-deficient mosquitoes. We found that only 20% of mice (n=10) bitten by Lp-depleted mosquitoes became blood-stage positive, as compared to 90% in

108 controls (n=10) (Figure 3A and 3B). To assure that this striking difference in infection
109 levels was not due to the differences in sporozoite loads produced by control and Lp-
110 deficient mosquitoes (Figure 1D), naïve mice were subcutaneously injected with equal
111 numbers of sporozoites isolated from control and Lp-depleted mosquitoes. Again, fewer
112 than 40% of mice (n=18) injected with lipid-deprived sporozoites became infected as
113 compared to 100% in controls (n=16) (Figure 3C). All mice that became infected with
114 sporozoites from Lp-deficient mosquitoes displayed a 1-day delay in the onset of
115 parasitemia (Figure 3D). In addition, only half of the infected mice displayed the severe
116 neurological symptoms typical of experimental cerebral malaria (ECM), and there was a
117 significant delay in ECM development (Figure 3E) compared to control mice, which had
118 100% incidence of ECM. Overall, mosquito lipid deprivation resulted in a cumulative
119 loss of parasite virulence (Figure 3F). These results strongly suggest that disrupting lipid
120 transport in the mosquito impacts development of *Plasmodium* liver stages and reduces
121 the initial burden of blood stage parasites, thereby preventing initiation of severe forms of
122 the disease.

123

124 **Supplemental blood feeding rescues parasite infectivity**

125 To obtain direct evidence of the trans-stadial effect of mosquito lipid deficiency on the
126 *Plasmodium* liver stages, we gauged development of extra-erythrocytic forms (EEFs) in
127 the hepatoma HepG2 cell line *in vitro*. Cells were exposed to equal numbers of
128 sporozoites isolated from control and Lp-depleted mosquitoes (Figure 4A) and the
129 development of EEFs was analyzed by fluorescence microscopy two days later.
130 Consistent with the *in vivo* results, lipid restriction reduced sporozoite infectivity in
131 hepatocytes 4-fold, to levels comparable to those observed after treatment of control
132 sporozoites with cytochalasin D, a potent inhibitor of actin polymerization and
133 *Plasmodium* invasion (Mota et al., 2001) (Figure 4C). Moreover, significantly smaller
134 EEFs were produced by lipid-deprived sporozoites as compared to controls (Figure 4E
135 and G, Figure S3), suggesting a trans-stadial effect of lipid deficiency on EEF growth.
136 Therefore, we hypothesized that providing lipids directly to the midgut at the critical time
137 of oocyst sporogony might restore sporozoite infectivity and EEF development. To test

138 this hypothesis, *P. berghei*-infected control and Lp-depleted mosquitoes were blood fed 7
139 dpi, when the first effects of lipid starvation on oocyst size were observed (Figure 2A).
140 Strikingly, even in the absence of Lp (Figure S4), this supplemental feeding partially
141 restored sporozoite numbers in the mosquitoes (Figure 4B), and fully rescued sporozoite
142 infectivity (Figure 4D) and EEF development (Figure 4F and H). As expected, additional
143 blood feeding did not restore ovary development (data not shown), confirming the
144 importance of Lp in lipid trafficking between mosquito organs. Taken together, these
145 results establish a direct link between lipid starvation at the oocyst stage and *Plasmodium*
146 infectivity to the next mammalian host.

147

148 **Mosquito lipids fuel sporozoite mitochondrial membrane potential**

149 We next examined potential mechanisms that attenuate sporozoite infectivity to the next
150 mammalian host. Microscopic inspection of the overall sporozoite morphology by
151 scanning electron microscopy failed to detect any major differences between control and
152 lipid-deficient sporozoites (Figure S5A). Similarly, no major differences were detected in
153 transcript levels of major regulators of sporozoite development (Figure S5B). Since
154 neutral lipids such as cholesterol regulate trafficking of GPI-anchored proteins to the
155 plasma membrane (Zurzolo and Simons, 2016), we gauged surface distribution of the
156 circumsporozoite protein (CSP), the main surface antigen crucial for sporozoite
157 morphogenesis and infectivity (Menard et al., 1997). Immunofluorescence analysis
158 revealed no differences in the distribution of CSP signal at the surface of lipid-deprived
159 sporozoites compared to controls (Figure S5C). In contrast, a striking effect of lipid
160 deprivation was observed on the sporozoite mitochondrial membrane potential as
161 measured by signal intensity of a lipophilic cationic dye (TMRE) whose accumulation in
162 the mitochondrial membrane matrix space correlates with the mitochondrial membrane
163 potential (Perry et al., 2011). We first validated TMRE staining of sporozoites by
164 measuring signal intensity before and after treatment with a mitochondrial uncoupling
165 drug CCCP and showed that drug treatment abolished TMRE signal (Figure S5D). We
166 next assessed TMRE intensity by imaging flow cytometry analysis of sporozoites.
167 Strikingly, a significant decrease in mitochondrial membrane potential was observed in

168 lipid-deprived sporozoites as compared to controls (Figure 5A, B and D). To examine
169 whether reduced mitochondrial activity mitigated sporozoite survival, we gauged levels
170 of transgenic GFP expression as a proxy of parasite live status (Yilmaz et al., 2014).
171 Although GFP expression levels differed between experiments, absence of significant
172 differences in GFP signal between the two groups confirmed that all analyzed sporozoites
173 were alive (Figure 5A, C and E). These results demonstrate that mosquito lipids regulate
174 the mitochondrial activity of sporozoites, and suggest that the decrease in mitochondrial
175 membrane potential is responsible for the attenuated infectivity of the lipid-deprived
176 sporozoites in the mammalian host.

177

178 **DISCUSSION**

179 Anopheline mosquitoes provide *Plasmodium* parasites a nutritional niche to complete
180 their life cycle. Here we report the crucial role of mosquito lipids in *Plasmodium*
181 metabolism that ultimately regulates parasite infectivity and virulence in the mammalian
182 host. We show that parasites hijack the mosquito nutrient transporter Lp for oocyst
183 provision with neutral lipids. These results are in line with previous reports that observed
184 an association of insect Lp particles with Apicomplexan parasites (Atella et al., 2009;
185 Folly et al., 2003; Ximenes Ados et al., 2015). We demonstrate that mosquito lipids
186 regulate multiple stages of *Plasmodium* development. First morphological anomalies
187 were detected during oocyst sporogony and were mainly characterized by electron-light
188 cytoplasmic vacuolization. Vacuolization is a hallmark of autophagy, a physiological
189 process occurring in normal conditions in a large proportion of *Plasmodium* liver stages
190 (Eickel et al., 2013). Indeed, under unfavorable circumstances such as starvation, liver
191 stage parasites initiate an autophagy-like cell death to reduce competition and ensure the
192 survival of the fittest progeny (Eickel et al., 2013). As in our experiments, a small
193 proportion of oocysts also displayed similar abnormalities in controls, we propose that
194 autophagy is not restricted to the intracellular liver stages, but is a general mechanism of
195 parasite nutrient sensing, exacerbated in our experiments by lipid restriction. Together
196 with the data accumulated for mammalian stages (Grellier et al., 1991; Itoe et al., 2014;
197 Lauer et al., 2000; Sa et al., 2017), our study uncovers the obligatory *Plasmodium*

198 dependence on host lipids during throughout its life cycle.

199 In contrast to sporogonic development, lipid restriction did not induce major
200 morphological or transcriptional changes in the transmissible sporozoite stage. Instead,
201 we revealed an unexpected association between mosquito lipid transport and sporozoite
202 mitochondrial membrane potential. Mitochondria are essential eukaryotic organelles that
203 integrate cellular metabolic signals, generate energy and synthetize intermediates of vital
204 macromolecules. In line with our results, *Plasmodium* mutants for mitochondrial
205 pathways are defective in oocyst growth and sporulation (Boysen and Matuschewski,
206 2011; Goodman et al., 2016; Hino et al., 2012; Oppenheim et al., 2014). Moreover, the
207 widely used antimalarial drug atovaquone, which targets the cytochrome bc1 complex
208 and collapses the mitochondrial membrane potential in *Plasmodium* blood stages (Siregar
209 et al., 2015; Srivastava et al., 1997) also arrests oocyst growth and sporulation, and
210 reduces the number and size of developing EEFs *in vitro* (Azevedo et al., 2017; Davies et
211 al., 1993; Fowler et al., 1995). Taken together with these results, our findings establish
212 the crucial role of mosquito lipids in parasite mitochondrial function, which shapes
213 *Plasmodium* sporogonic development and infectivity.

214 Attenuation of *Plasmodium* sporozoites is a leading strategy for malaria whole-organism
215 vaccine development (Butler et al., 2012). So far, this has been achieved by irradiation
216 (Seder et al., 2013) or by genetic manipulation (van Schaijk et al., 2014). The data
217 presented here add a new paradigm of virulence attenuation by manipulation of mosquito
218 lipid trafficking. Interestingly, high variability in virulence of *P. falciparum* sporozoites
219 has been reported under laboratory conditions (March et al., 2013) and in the field (Gupta
220 et al., 1994; Mackinnon and Read, 2004). We propose that disparity in lipid resources
221 between larval breeding sites drive fluctuations in mosquito nutritional status (Gillies,
222 1954), and thereby may account for the observed variability in *Plasmodium* virulence in
223 the field. Therefore, the demonstrated direct correlation between sporozoite quantities
224 and transmission efficiency in naïve and vaccinated hosts (Churcher et al., 2017) should
225 also consider sporozoite quality, both of which depend on the mosquito nutritional status.
226 Finally, targeting host/vector lipid trafficking may offer new potent and powerful
227 strategies to block parasite development in the next host, thereby preventing the vicious

228 cycle of malaria transmission.

229

230 **AUTHOR CONTRIBUTIONS**

231 GC and EAL conceived the study and designed the experiments. GC, ME, RL, CG, and
232 VB performed experiments. AEH and RS contributed reagents and expertise. GC, ME,
233 RL, RS, CG, VB, and EAL analyzed the data. GC and EAL wrote the manuscript.

234

235

236 **ACKNOWLEDGEMENTS**

237

238 This work was supported by EC FP7 EVIMalaR (grant agreement n°242095) and
239 MALVECBLOK (grant agreement nº223601). The authors thank H. Krüger, M. Andres
240 and L. Spohr for mosquito rearing, mouse work assistance, and *Plasmodium* infections,
241 and D. Tschierske and D. Eyermann for *P. falciparum* cultures. Editorial support of Dr.
242 R. Willmott (Bioscript) is gratefully acknowledged. The authors express their gratitude to
243 Prof. K. Matuschewski and his group for continuous fruitful discussions and to Dr. M.M.
244 Mota for helpful comments.

245 **REFERENCES:**

246

247 Atella, G.C., Bittencourt-Cunha, P.R., Nunes, R.D., Shahabuddin, M., and Silva-Neto,
248 M.A. (2009). The major insect lipoprotein is a lipid source to mosquito stages of malaria
249 parasite. Acta Trop *109*, 159-162.

250 Atella, G.C., Silva-Neto, M.A., Golodne, D.M., Arefin, S., and Shahabuddin, M. (2006).
251 *Anopheles gambiae* lipophorin: characterization and role in lipid transport to developing
252 oocyte. Insect Biochem Mol Biol *36*, 375-386.

253 Azevedo, R., Markovic, M., Machado, M., Franke-Fayard, B., Mendes, A.M., and
254 Prudencio, M. (2017). A bioluminescence method for in vitro screening of Plasmodium
255 transmission-blocking compounds. Antimicrob Agents Chemother.

256 Boysen, K.E., and Matuschewski, K. (2011). Arrested oocyst maturation in Plasmodium
257 parasites lacking type II NADH:ubiquinone dehydrogenase. J Biol Chem *286*, 32661-
258 32671.

259 Butler, N.S., Vaughan, A.M., Harty, J.T., and Kappe, S.H. (2012). Whole parasite
260 vaccination approaches for prevention of malaria infection. Trends Immunol *33*, 247-254.

261 Carroll, R.W., Wainwright, M.S., Kim, K.Y., Kidambi, T., Gomez, N.D., Taylor, T., and
262 Haldar, K. (2010). A rapid murine coma and behavior scale for quantitative assessment of
263 murine cerebral malaria. PLoS One *5*.

264 Churcher, T.S., Sinden, R.E., Edwards, N.J., Poulton, I.D., Rampling, T.W., Brock, P.M.,
265 Griffin, J.T., Upton, L.M., Zakutansky, S.E., Sala, K.A.*, et al.* (2017). Probability of
266 Transmission of Malaria from Mosquito to Human Is Regulated by Mosquito Parasite
267 Density in Naive and Vaccinated Hosts. PLoS Pathog *13*, e1006108.

268 Coppi, A., Tewari, R., Bishop, J.R., Bennett, B.L., Lawrence, R., Esko, J.D., Billker, O.,
269 and Sinnis, P. (2007). Heparan sulfate proteoglycans provide a signal to Plasmodium
270 sporozoites to stop migrating and productively invade host cells. Cell Host Microbe *2*,
271 316-327.

272 Davies, C.S., Pudney, M., Nicholas, J.C., and Sinden, R.E. (1993). The novel
273 hydroxynaphthoquinone 566C80 inhibits the development of liver stages of Plasmodium
274 berghei cultured in vitro. Parasitology *106 (Pt 1)*, 1-6.

275 Eickel, N., Kaiser, G., Prado, M., Burda, P.C., Roelli, M., Stanway, R.R., and Heussler,
276 V.T. (2013). Features of autophagic cell death in Plasmodium liver-stage parasites.
277 Autophagy *9*, 568-580.

278 Folly, E., Cunha e Silva, N.L., Lopes, A.H., Silva-Neto, M.A., and Atella, G.C. (2003).
279 Trypanosoma rangeli uptakes the main lipoprotein from the hemolymph of its
280 invertebrate host. Biochem Biophys Res Commun *310*, 555-561.

281 Fowler, R.E., Sinden, R.E., and Pudney, M. (1995). Inhibitory activity of the anti-
282 malarial atovaquone (566C80) against ookinetes, oocysts, and sporozoites of Plasmodium
283 berghei. J Parasitol *81*, 452-458.

284 Franke-Fayard, B., Trueman, H., Ramesar, J., Mendoza, J., van der Keur, M., van der
285 Linden, R., Sinden, R.E., Waters, A.P., and Janse, C.J. (2004). A *Plasmodium berghei*
286 reference line that constitutively expresses GFP at a high level throughout the complete
287 life cycle. Mol Biochem Parasitol *137*, 23-33.

288 Gillies, M.T. (1954). The recognition of age-groups within populations of *Anopheles*
289 *gambiae* by the pre-gravid rate and the sporozoite rate. Ann Trop Med Parasitol *48*, 58-
290 74.

291 Goodman, C.D., Siregar, J.E., Mollard, V., Vega-Rodriguez, J., Syafruddin, D.,
292 Matsuoka, H., Matsuzaki, M., Toyama, T., Sturm, A., Cozijnsen, A.*, et al.* (2016).
293 Parasites resistant to the antimalarial atovaquone fail to transmit by mosquitoes. Science
294 *352*, 349-353.

295 Grellier, P., Rigomier, D., Clavey, V., Fruchart, J., and Schrevel, J. (1991). Lipid Traffic
296 Between High Density Lipoproteins and *Plasmodium-falciparum*-Infected Red Blood
297 Cells. J Cell Biol *112*, 267-277.

298 Gupta, S., Hill, A.V.S., Kwiatkowski, D., Greenwood, A.M., Greenwood, B., and Day,
299 K. (1994). Parasite virulence and disease patterns in *Plasmodium falciparum* malaria.
300 Proc Natl Acad Sci U S A *91*, 3715-3719.

301 Hino, A., Hirai, M., Tanaka, T.Q., Watanabe, Y., Matsuoka, H., and Kita, K. (2012).
302 Critical roles of the mitochondrial complex II in oocyst formation of rodent malaria
303 parasite Plasmodium berghei. J Biochem *152*, 259-268.

304 Itoe, M.A., Sampaio, J.L., Cabal, G.G., Real, E., Zuzarte-Luis, V., March, S., Bhatia,
305 S.N., Frischknecht, F., Thiele, C., Shevchenko, A.*, et al.* (2014). Host cell
306 phosphatidylcholine is a key mediator of malaria parasite survival during liver stage
307 infection. Cell Host Microbe *16*, 778-786.

308 Lackner, P., Beer, R., Heussler, V., Goebel, G., Rudzki, D., Helbok, R., Tannich, E., and
309 Schmutzhard, E. (2006). Behavioural and histopathological alterations in mice with
310 cerebral malaria. Neuropathol Appl Neurobiol *32*, 177-188.

311 Lauer, S., VanWye, J., Harrison, T., McManus, H., Samuel, B.U., Hiller, N.L.,
312 Mohandas, N., and Haldar, K. (2000). Vacuolar uptake of host components, and a role for
313 cholesterol and sphingomyelin in malarial infection. EMBO J *19*, 3556-3564.

314 Mackinnon, M.J., and Read, A.F. (2004). Immunity promotes virulence evolution in a
315 malaria model. PLoS Biol *2*, E230.

316 March, S., Ng, S., Velmurugan, S., Galstian, A., Shan, J., Logan, D.J., Carpenter, A.E.,
317 Thomas, D., Sim, B.K., Mota, M.M*., et al.* (2013). A microscale human liver platform
318 that supports the hepatic stages of *Plasmodium falciparum* and *vivax*. Cell Host Microbe
319 *14*, 104-115.

320 Menard, R., Sultan, A.A., Cortes, C., Altszuler, R., van Dijk, M.R., Janse, C.J., Waters,
321 A.P., Nussenzweig, R.S., and Nussenzweig, V. (1997). Circumsporozoite protein is
322 required for development of malaria sporozoites in mosquitoes. Nature *385*, 336-340.

323 Mendes, A.M., Schlegelmilch, T., Cohuet, A., Awono-Ambene, P., De Iorio, M.,
324 Fontenille, D., Morlais, I., Christophides, G.K., Kafatos, F.C., and Vlachou, D. (2008).
325 Conserved mosquito/parasite interactions affect development of *Plasmodium falciparum*
326 in Africa. PLoS Pathog *4*, e1000069.

327 Moller-Jacobs, L.L., Murdock, C.C., and Thomas, M.B. (2014). Capacity of mosquitoes
328 to transmit malaria depends on larval environment. Parasites & vectors *7*, 593.

329 Mota, M.M., Pradel, G., Vanderberg, J.P., Hafalla, J.C., Frevert, U., Nussenzweig, R.S.,
330 Nussenzweig, V., and Rodriguez, A. (2001). Migration of *Plasmodium* sporozoites
331 through cells before infection. Science *291*, 141-144.

332 Muller, K., Matuschewski, K., and Silvie, O. (2011). The Puf-family RNA-binding
333 protein Puf2 controls sporozoite conversion to liver stages in the malaria parasite. PloS
334 one *6*, e19860.

335 Okech, B.A., Gouagna, L.C., Kabiru, E.W., Beier, J.C., Yan, G., and Githure, J.I. (2004).
336 Influence of age and previous diet of *Anopheles gambiae* on the infectivity of natural
337 *Plasmodium falciparum* gametocytes from human volunteers. Journal of insect science *4*,
338 33.

339 Oppenheim, R.D., Creek, D.J., Macrae, J.I., Modrzynska, K.K., Pino, P., Limenitakis, J.,
340 Polonais, V., Seeber, F., Barrett, M.P., Billker, O*., et al.* (2014). BCKDH: the missing
341 link in apicomplexan mitochondrial metabolism is required for full virulence of
342 Toxoplasma gondii and Plasmodium berghei. PLoS Pathog *10*, e1004263.

343 Perry, S.W., Norman, J.P., Barbieri, J., Brown, E.B., and Gelbard, H.A. (2011).
344 Mitochondrial membrane potential probes and the proton gradient: a practical usage
345 guide. BioTechniques *50*, 98-115.

346 Pompon, J., and Levashina, E.A. (2015). A New Role of the Mosquito Complement-like
347 Cascade in Male Fertility in *Anopheles gambiae*. PLoS Biol *13*, e1002255.

348 Ponnudurai, T., Lensen, A.H., van Gemert, G.J., Bensink, M.P., Bolmer, M., and
349 Meuwissen, J.H. (1989). Sporozoite load of mosquitoes infected with *Plasmodium*
350 *falciparum*. Trans R Soc Trop Med Hyg *83*, 67-70.

351 Rono, M.K., Whitten, M.M., Oulad-Abdelghani, M., Levashina, E.A., and Marois, E.
352 (2010). The major yolk protein vitellogenin interferes with the anti-*Plasmodium* response
353 in the malaria mosquito *Anopheles gambiae*. PLoS Biol *8*, e1000434.

354 Rudolf, M., and Curcio, C.A. (2009). Esterified cholesterol is highly localized to Bruch's
355 membrane, as revealed by lipid histochemistry in wholemounts of human choroid. J
356 Histochem Cytochem *57*, 731-739.

357 Sa, E.C.C., Nyboer, B., Heiss, K., Sanches-Vaz, M., Fontinha, D., Wiedtke, E., Grimm,
358 D., Przyborski, J.M., Mota, M.M., Prudencio, M.*, et al.* (2017). Plasmodium berghei
359 EXP-1 interacts with host Apolipoprotein H during Plasmodium liver-stage development.
360 Proc Natl Acad Sci U S A *114*, E1138-E1147.

361 Seder, R.A., Chang, L.J., Enama, M.E., Zephir, K.L., Sarwar, U.N., Gordon, I.J.,
362 Holman, L.A., James, E.R., Billingsley, P.F., Gunasekera, A.*, et al.* (2013). Protection
363 against malaria by intravenous immunization with a nonreplicating sporozoite vaccine.
364 Science *341*, 1359-1365.

365 Shapiro, L.L., Murdock, C.C., Jacobs, G.R., Thomas, R.J., and Thomas, M.B. (2016).
366 Larval food quantity affects the capacity of adult mosquitoes to transmit human malaria.
367 Proc Biol Sci *283*.

368 Shiao, S.H., Whitten, M.M., Zachary, D., Hoffmann, J.A., and Levashina, E.A. (2006).
369 *Fz2* and *cdc42* mediate melanization and actin polymerization but are dispensable for
370 *Plasmodium* killing in the mosquito midgut. PLoS Pathog *2*, e133.

371 Silvie, O., Goetz, K., and Matuschewski, K. (2008). A sporozoite asparagine-rich protein
372 controls initiation of *Plasmodium* liver stage development. PLoS Pathog *4*, e1000086.

373 Siregar, J.E., Kurisu, G., Kobayashi, T., Matsuzaki, M., Sakamoto, K., Mi-ichi, F.,
374 Watanabe, Y., Hirai, M., Matsuoka, H., Syafruddin, D.*, et al.* (2015). Direct evidence for

375 the atovaquone action on the Plasmodium cytochrome bc1 complex. Parasitol Int *64*,
376 295-300.

377 Srivastava, I.K., Rottenberg, H., and Vaidya, A.B. (1997). Atovaquone, a broad spectrum
378 antiparasitic drug, collapses mitochondrial membrane potential in a malarial parasite. J
379 Biol Chem *272*, 3961-3966.

380 Takken, W., Smallegange, R.C., Vigneau, A.J., Johnston, V., Brown, M., Mordue-Luntz,
381 A.J., and Billingsley, P.F. (2013). Larval nutrition differentially affects adult fitness and
382 *Plasmodium* development in the malaria vectors *Anopheles gambiae* and *Anopheles*
383 *stephensi*. Parasites & vectors *6*, 345.

384 Van der Horst, D.J., Roosendaal, S.D., and Rodenburg, K.W. (2009). Circulatory lipid
385 transport: lipoprotein assembly and function from an evolutionary perspective. Mol Cell
386 Biochem *326*, 105-119.

387 van Schaijk, B.C., Ploemen, I.H., Annoura, T., Vos, M.W., Foquet, L., van Gemert, G.J.,
388 Chevalley-Maurel, S., van de Vegte-Bolmer, M., Sajid, M., Franetich, J.F*., et al.* (2014).
389 A genetically attenuated malaria vaccine candidate based on *P. falciparum* b9/slarp gene-
390 deficient sporozoites. eLife *3*.

391 Vantaux, A., Lefevre, T., Cohuet, A., Dabire, K.R., Roche, B., and Roux, O. (2016).
392 Larval nutritional stress affects vector life history traits and human malaria transmission.
393 Sci Rep *6*, 36778.

394 Ximenes Ados, A., Silva-Cardoso, L., De Cicco, N.N., Pereira, M.G., Lourenco, D.C.,
395 Fampa, P., Folly, E., Cunha-e-Silva, N.L., Silva-Neto, M.A., and Atella, G.C. (2015).
396 Lipophorin Drives Lipid Incorporation and Metabolism in Insect Trypanosomatids.
397 Protist *166*, 297-309.

398 Yilmaz, B., Portugal, S., Tran, T.M., Gozzelino, R., Ramos, S., Gomes, J., Regalado, A.,
399 Cowan, P.J., d'Apice, A.J., Chong, A.S*., et al.* (2014). Gut microbiota elicits a protective
400 immune response against malaria transmission. Cell *159*, 1277-1289.

401 Yuda, M., Iwanaga, S., Shigenobu, S., Kato, T., and Kaneko, I. (2010). Transcription
402 factor AP2-Sp and its target genes in malarial sporozoites. Mol Microbiol *75*, 854-863.
403 Zurzolo, C., and Simons, K. (2016). Glycosylphosphatidylinositol-anchored proteins:
404 Membrane organization and transport. Biochim Biophys Acta *1858*, 632-639.
405
406 Zurzolo, C., and Simons, K. (2016). Glycosylphosphatidylinositol-anchored proteins:
407 Membrane organization and transport. Biochim Biophys Acta *1858*, 632-639.
408
409

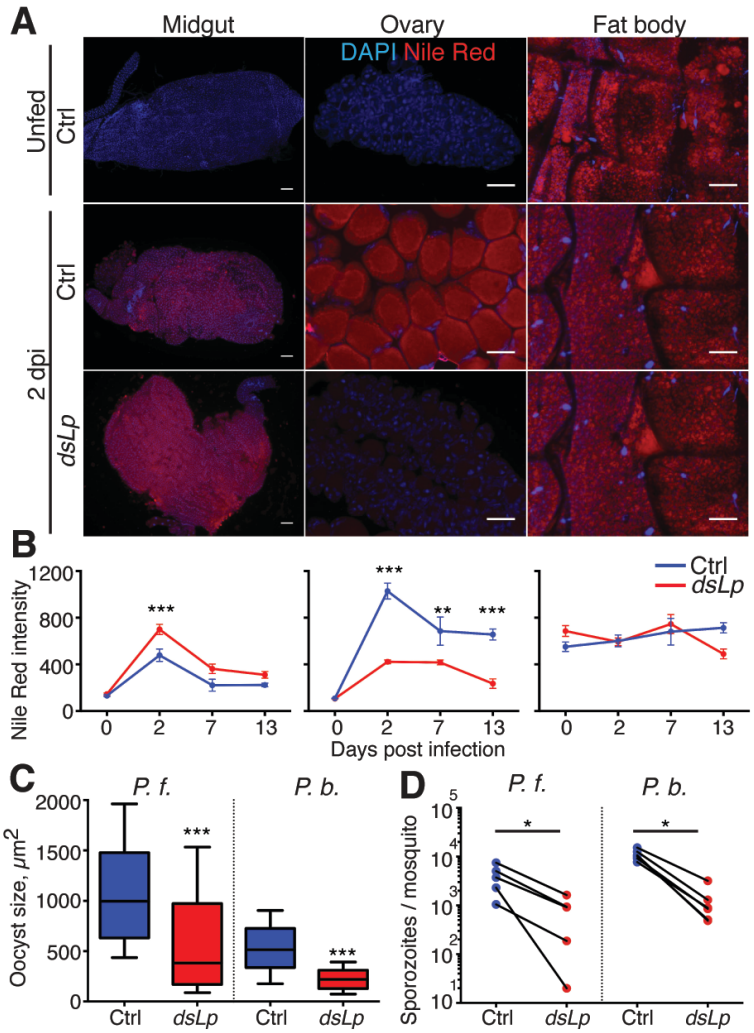

Figure 1. Effect of mosquito lipid trafficking on *Plasmodium* sporogony.

Distribution of neutral lipids (Nile Red dye) in the midgut, ovaries, and fat body of control (Ctrl) and Lp-deficient (*dsLp*) mosquitoes. (**A**) Representative fluorescence micrographs of female abdomens of control and Lp-depleted mosquitoes dissected before (unfed), 2, 7 and 13 days post *Plasmodium* infection (dpi). Neutral lipids are stained by Nile Red (red) and cell nuclei are in blue (DAPI). Scale bar - 100 µm. (**B**) Intensity of the Nile Red staining was measured in the midgut, ovaries, and fat body of control and Lp-depleted mosquitoes. Each data point represents the mean intensity of Nile Red signal ± SEM per midgut (n≥3). Control and Lp-deficient females were infected with *P. falciparum* (*P.f.)* or *P. berghei* (*P.b.*). (**C**) Sizes of *P.f.* (11 dpi, n=3) and *P.b.* (14 dpi, n=6) oocysts in control and Lp-depleted mosquitoes. At least 225 oocysts were measured

423 per condition. The box plots represent medians (horizontal bars) with 10th and 90th
424 percentiles. (**D**) Development of *P.f.* (14 dpi, n=5) and *P.b.* (18 dpi, n=4) salivary gland
425 sporozoites in control and Lp-depleted mosquitoes. Each point represents the mean
426 number of sporozoites per mosquito for each experimental replicate. Asterisks indicate
427 statistically significant differences (Mann-Whitney test and 2-way ANOVA, *$p<0.05$;
428 **$p<0.001$; ***$p<0.0001$).
429

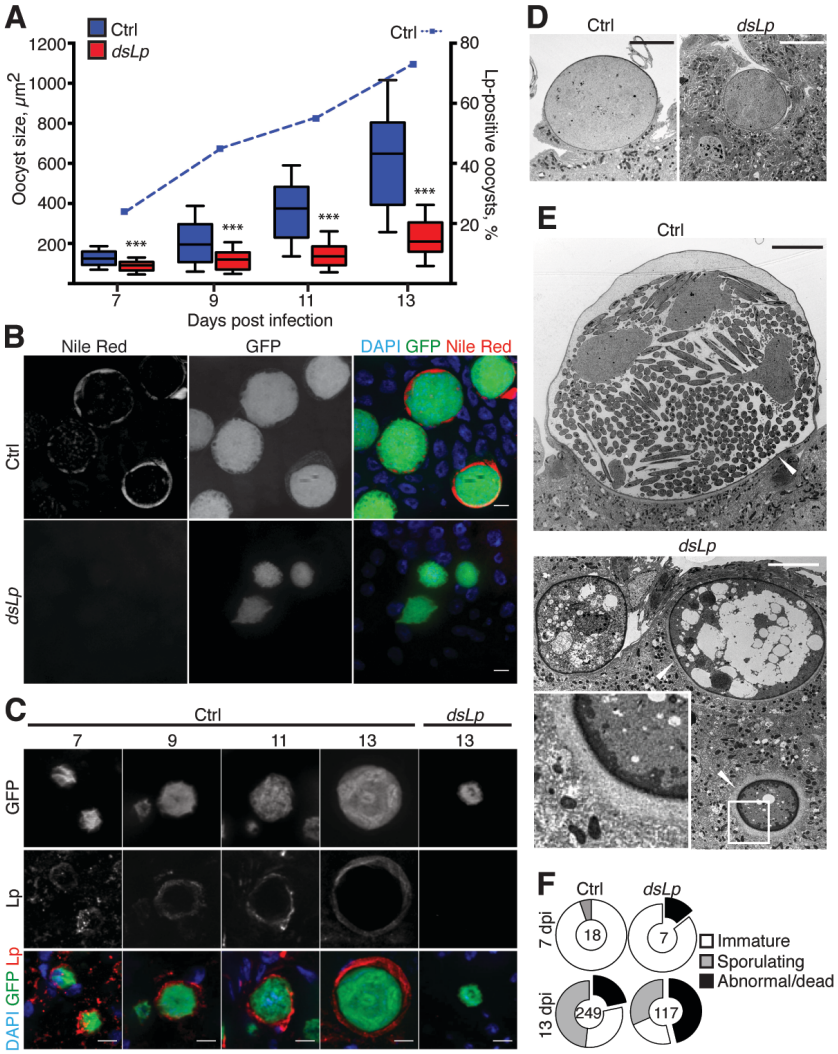

Figure 2. Disruption of mosquito lipid trafficking impairs *Plasmodium* sporogony. Control (Ctrl) and Lp-deficient (*dsLp*) females were infected with *P. berghei* and the oocyst sizes, morphology, lipid, and Lp uptake were gauged by fluorescence and transmission electron microscopy. (**A**) Time-series analysis of oocyst development in control (blue) and Lp-depleted (red) mosquitoes. At least 5 mosquitoes were dissected per time point and per condition (n=2). The box plots represent medians (horizontal bars) with 10th and 90th percentiles. (**B**) Neutral lipids (red) detected by the Nile Red dye inside the GFP-expressing *P. berghei* oocysts (green) 14 dpi in control and Lp-depleted mosquitoes. Nuclei are visualized by DAPI (blue). Scale bars - 10 μm. (**C**) Lp accumulation (red) on the GFP-expressing oocysts (green) in the midguts of control *P. berghei*-infected mosquitoes revealed by immunofluorescence analysis using anti-Lp

442 antibodies at 7, 9, 11, and 13 days post infection (dpi). No Lp signal was observed in Lp-
443 depleted mosquitoes. Nuclei are visualized by DAPI (blue). Scale bars - 10 µm.
444 Representative transmission electron micrographs of *P. berghei* oocysts in control and
445 Lp-depleted mosquitoes 7 (**D**) and 13 (**E**) dpi. White arrowheads point to the
446 membranous structures in control and to the electron-dense actin-zone in Lp-depleted
447 mosquitoes. Scale bars - 10 µm. (**F**) Oocysts detected by transmission electron
448 microscopy were scored according to the developmental stage: non-sporulating oocysts
449 with normal morphology (immature, white); oocysts with normal plasma membrane
450 retraction, budding sporoblasts, or formed sporozoites (sporulating, gray); oocysts with
451 aberrant electron-light intracellular vacuolization (abnormal/dead, black). Proportions of
452 the categories are shown as pie charts and the total numbers of analyzed oocysts per
453 condition are indicated in the middle of each chart. Asterisks indicate statistically
454 significant differences (Kruskal-Wallis test, ***$p<0.0001$).

455

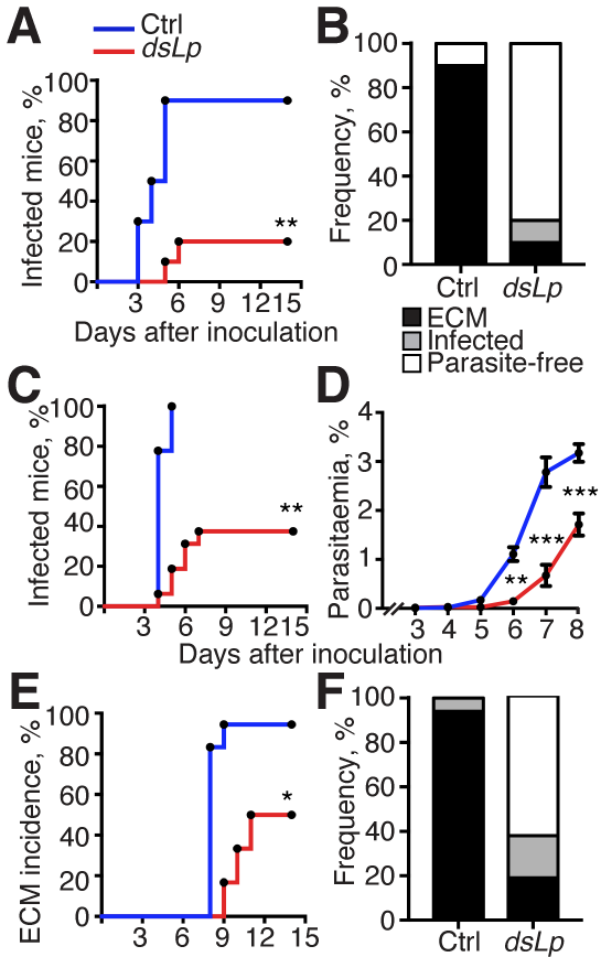

Figure 3. Mosquito lipids determine *Plasmodium* virulence in mammalian hosts. C57BL/6 mice were infected with *P. berghei* and monitored daily for parasite occurrence in the blood by Giemsa staining of thin blood smears and by FACS and experimental cerebral malaria symptoms (ECM) malaria symptoms. (**A**) Kaplan-Meier analysis of time to malaria and (B) cumulative health status frequencies of mice infected by control (CTRL, blue line, n=10) or Lp-depleted (*dsLp*, red line, n=10) mosquitoes via direct bite. (**C**) Kaplan-Meier analysis of time to malaria, (D) means and SEM of parasitemia, (E) percentage of experimental cerebral malaria (ECM) incidence and (F) cumulative health status frequencies of mice infected by subcutaneous injection of 5,000 sporozoites dissected from the salivary glands of control (CTRL, blue line, n=18) or Lp-depleted (*dsLp*, red line, n=16) mosquitoes. Asterisks indicate statistically significant differences (log-rank Mantel-Cox test and 2-way ANOVA *p<0.05; **p<0.001, ***p<0.0001.

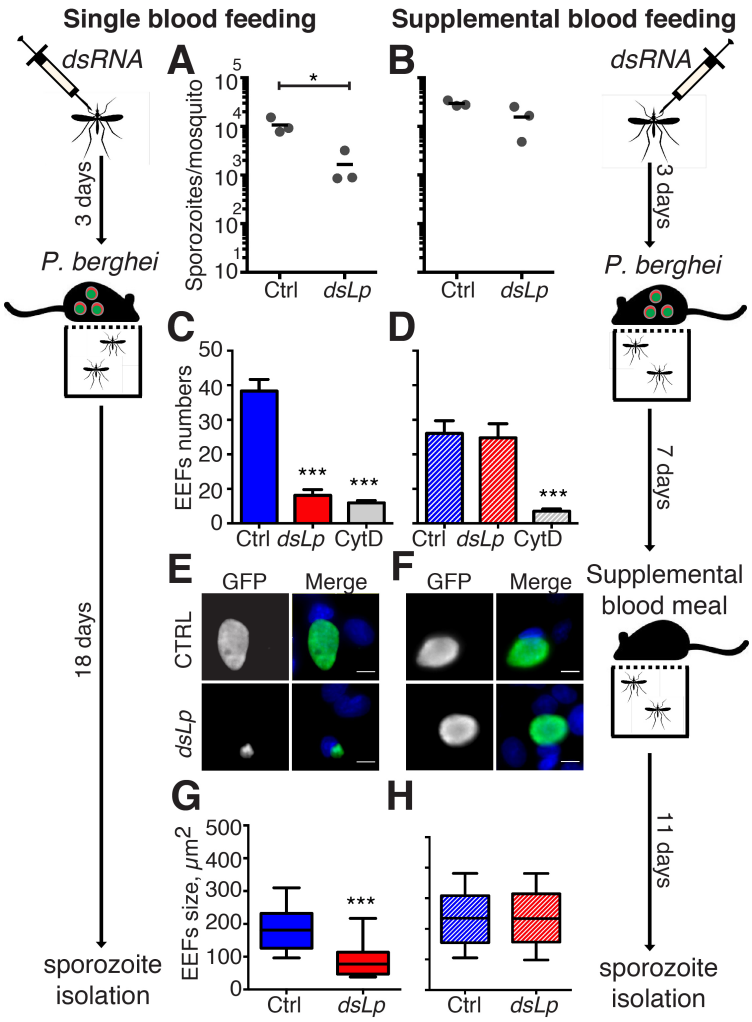

Figure 4. Mosquito lipids attenuate sporozoite infectivity to hepatocytes.

Lp-depleted mosquitoes (*dsLp*) and controls (CTRL) were infected with *P. berghei* and offered (**B, D, F and H**) or not (**A, C, E and G**) a supplemental blood meal 7 days post infection. (**A** and **B**) Salivary gland sporozoites were isolated and counted from control and Lp-deficient mosquitoes. (**C** and **D**) Human hepatoma HepG2 cells were infected with 10,000 sporozoites and the number of extra-erythrocytic forms (EEFs) per field was gauged by microscopy 2 dpi. As a negative control, sporozoites from control mosquitoes were treated with cytochalasin D (Cyt D). Mean numbers and SEM are shown. (**E** and **F**) Representative fluorescent micrographs of GFP-expressing EEFs (green) developing in HepG2 cells. Cell nuclei are stained with DAPI (blue). Scale bar - 10 µm. (**G** and **H**) EEF

485 sizes produced by sporozoites from control and Lp-deficient mosquitoes. The box plots
486 represent 10th and 90th percentiles while the horizontal lines show medians. Asterisks
487 indicate statistically significant differences (n=3, Kruskal-Wallis and Mann-Whitney test,
488 *$p<0.05$; ***$p<0.0001$).

489

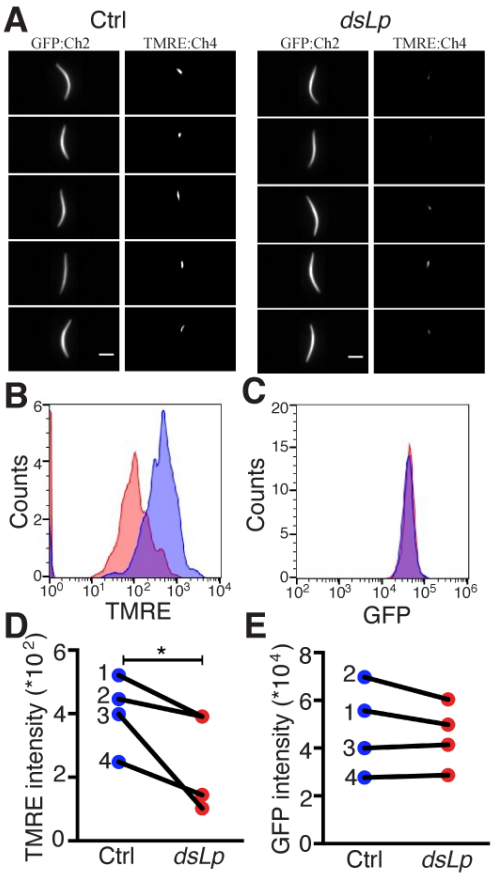

Figure 5. Mosquito lipids regulate sporozoite mitochondrial membrane potential. (**A**) Sporozoite GFP expression and mitochondrial membrane potential as measured by TMRE staining were analysed using imaging flow cytometry. Representative images of control (Ctrl) and lipid-deprived (*dsLp*) sporozoites are shown. Scale bars - 5 µm. Histograms from one representative experiment (3, 270 events per condition) showing (**B**) TMRE signal (Bright Detail Intensity R7 of Channel 4) or (**C**) GFP (Intensity MC of Channel 2) in control (blue) and lipid-deprived (red) sporozoites. Geometrical mean values of (**D**) Bright Detail Intensity R7 of Channel 4 or (**E**) Intensity MC of Channel 2 from four independent experiments in control (blue, N=1405) and lipid-deprived (red, N=593) sporozoites. Asterisks indicate statistically significant differences (Paired t test, *p<0.05).

504 **EXPERIMENTAL PROCEDURES**

505 **Mosquito Rearing and Parasite Infections**

506 *Anopheles gambiae s.l.* mosquitoes were used throughout the study. G3 and 7b lines - an
507 immunocompromised transgenic mosquito line of G3 origin in which expression of the
508 complement-like gene TEP1 is down-regulated (Pompon and Levashina, 2015), were
509 maintained at 29°C 70%–80% humidity 12/12 h day/night cycle. In *P. falciparum*
510 infections, mosquitoes were fed at 37°C for 15 min through a membrane feeder with
511 NF54 gametocytes cultured with O+ human red blood cells (Haema, Berlin), and
512 thereafter kept in a secured S3 laboratory according to the national regulations
513 (Landesamt für Gesundheit und Soziales, project number 411/08). For *P. berghei*
514 experiments, mosquitoes were fed on anesthetized CD1 mice infected with the *P. berghei*
515 GFP-con 259cl2 clone (ANKA strain) that constitutively expresses GFP (Franke-Fayard
516 et al., 2004). Shortly after infections, unfed mosquitoes were removed, while fed
517 mosquitoes were maintained at 26°C for 11-14 days (*P. falciparum*) or at 20°C for 7-21
518 days (*P. berghei*), and then used for the midgut and/or the salivary gland dissections.

519

520 **RNAi silencing**

521 Double stranded RNA (dsRNA) against *lipophorin* (*dsLp*) was produced as previously
522 described (Rono et al., 2010). For RNAi silencing, 1-2 day-old females were anesthetized
523 with CO_2 and injected with 69 nl of 3 µg/µl *dsLacZ* (control) or *dsLp* using a Nanoject II
524 Injector (Drummond). Mosquitoes recovered for 3-4 days following injection before
525 infections. Efficiencies of RNAi silencing are summarized in Figure S5.

526

527 **Immunofluorescence Analysis**

528 Mosquito midguts were dissected in PBS, fixed in 4% formaldehyde and washed in PBS.
529 Tissues were permeabilized with Triton X-100 0.1% and incubated with a 1:1 mix of
530 mouse monoclonal anti-ApoI and anti-ApoII antibodies (1/300, clones 2H5 and 2C6)

531 (Rono et al., 2010) overnight at 4°C followed by incubation for 40 min at room
532 temperature with the secondary Cy3-labeled antibodies at 1/1,000 (Molecular Probes), or
533 with 0.1 µg/ml of the Nile Red dye (Sigma Aldrich). Nuclei were stained with DAPI
534 (1.25 µg/ml, Molecular Probes) for 40-60 min at room temperature. Images were
535 acquired using an AxioObserver Z1 fluorescence microscope equipped with an Apotome
536 module (Zeiss). Oocyst sizes were measured by hand-designing a circular ROI of
537 randomly selected oocysts (identified by GFP for *P. berghei* or by bright field and DAPI
538 staining for *P. falciparum*) using ZEN 2012 software (Zeiss). Images were then processed
539 by FIJI software (ImageJ 1.47m).

540

541 **Transmission and Scanning Electron Microscopy**

542 Infected midguts were dissected in PBS, embedded in a drop of low melting agarose (4%)
543 and fixed overnight in 2.5% EM grade glutaraldehyde at 4°C. Midguts were postfixed in
544 0.5% osmium tetroxide, contrasted with tannic acid and 2% uranyl acetate, dehydrated,
545 and embedded in epoxy resin. After polymerization, sections were cut at 60 nm and
546 contrasted with lead citrate. Specimens were analyzed in a Leo 906E transmission
547 electron microscope at 100KV (Zeiss) using digital camera (Morada).

548

549 ***P. berghei* liver-stage development *in vitro***

550 The salivary glands and midguts of *P. berghei* infected mosquitoes were dissected,
551 sporozoites were collected into RPMI medium (Gibco) 3% bovine serum albumin (Sigma
552 Aldrich) and enumerated with a hemocytometer. The *P. berghei* liver stages were
553 cultured *in vitro* in HepG2 hepatoma cells and analyzed using standard techniques (Silvie
554 et al., 2008). In short, 15,000 - 20,000 HepG2 cells per well (70% confluence) were
555 plated in the transparent-bottom 96-wells plates (Nalgene International) and incubated for
556 24 h, then seeded with 10,000 sporozoites and left at 37°C for 2 h. Non-invading
557 sporozoites were removed by washing. As a negative control, sporozoites isolated from
558 control mosquitoes were pre-treated with the inhibitor of actin polymerization

559 Cytochalasin D (Sigma Aldrich) for 10 min. At 48 h post seeding, the cells were fixed for
560 10 min with 4% formaldehyde, washed with PBS and blocked with 10% fetal calf serum
561 in PBS. Development of the liver-stage parasites was examined using monoclonal mouse
562 anti-GFP antibodies (1/1,000, AbCam) and revealed with the secondary AlexaFluor488
563 conjugated anti-mouse antibody (1/1,000, Molecular Probes). Nuclei were stained with
564 DAPI (1.25 µg/ml, Molecular Probes). Images were recorded directly on the 96-wells
565 plate using an AxioObserver Z1 fluorescence microscope equipped with an Apotome
566 module (Zeiss) and analyzed for number and size of liver forms using the Axio-Vision
567 ZEN 2012 software (Zeiss).

568

569 ***P. berghei* mouse infections *in vivo***

570 Mice were housed and handled in accordance with the German Animal Protection Law
571 (§8 Tierschutzgesetz) and both institutional (Max Planck Society) and national
572 regulations (Landesamt für Gesundheit und Soziales, registration number H 0027/12). To
573 determine sporozoite infectivity to mice, the sporozoites collected from the mosquito
574 salivary glands (5,000 sporozoites/mouse) were injected subcutaneously into the tails of
575 8-10-week-old C57BL/6 females. Bite-back experiments were performed by feeding the
576 *P. berghei*-infected mosquitoes (18 dpi) on anesthetized naïve C57BL/6 mice (mean 9
577 bites/mouse, range 2-15). Blood cell parasitemia was determined by daily Giemsa
578 staining of thin blood smears and FACS analysis of the red blood cells with the GFP-
579 expressing blood stage parasites. Infected mice were monitored every 6-12 h for the
580 appearance of severe neurological and behavioral symptoms typical of experimental
581 cerebral malaria (ECM) such as hunched body position, grooming alteration, ataxia,
582 paralysis, or convulsions (Lackner et al., 2006) or by the rapid neurological and
583 behavioral test (RMCBS) (Carroll et al., 2010). All mice with ECM symptoms or the
584 RMCBS score equal or below 5/20 were sacrificed immediately.

585

586 **Sporozoite imaging flow cytometry**

587 Salivary gland sporozoites were purified in RPMI medium (Gibco) 3% bovine serum
588 albumin (Sigma Aldrich) and kept on ice until staining. Sporozoites were diluted in PBS
589 to concentrations corresponding to 3 mosquito equivalents and stained in the dark with 5
590 nM TMRE (Cell Signalling Technology) for 20 min at 20°C. CCCP at 50 µM was used
591 as a negative control (see Figure S5D). Sporozoite images were acquired without washing
592 using an ImageStreamX Mk II (Merck Millipore) with a 60x objective over 1 h period.
593 To avoid a possible bias due to the variable pre-acquisition waiting times on ice, the order
594 of sample acquisition was swapped in half of the experimental replicates. GFP-expressing
595 sporozoites were gated by size (Area_M01 or Area_M02) and by GFP intensity
596 (Intensity_MC_Ch02). The analysis was performed with IDEAS 6.2 (Merck Millipore)
597 and FCS files were exported and analyzed by FlowJo v10. Given the small size of the
598 sporozoite mitochondria, the feature finder tool from IDEAS software was used to
599 improve gating of optimally focused sporozoites. The following parameters were used to
600 discriminate focused single sporozoites from debris, and to identify sporozoites sharply
601 focused enough to resolve their mitochondria: H Entropy Std_M01_Ch01_15 over H
602 Variance Std_M01_Ch01, Aspect Ratio_M02 over Symmetry 4-Object(M02,Ch2)_Ch02,
603 Gradient RMS-M01-Ch01 over H Correlation Mean-M02-Ch02_3, and Gradient RMS-
604 M02_Ch02. Briefly, these parameters respectively measure brightfield image texture,
605 GFP image shape, and brightfield and GFP focus. For measurement of mitochondrial
606 membrane potential and GFP intensity, each sample was time-gated to exclude events
607 with prolonged live staining. The parameter corresponding to the lowest background
608 signal in unstained sporozoites was Bright Detail Intensity R7_M04_Ch04, Geo Mean
609 which was selected as *bona fide* TMRE intensity readout (see Figure S5D). For GFP
610 intensity the Intensity_MC_Ch02, Geo. Mean was used.

611

612 **Statistical analysis**

613 Statistical analysis were performed using GraphPad Prism 7 software and p values < 0.05
614 were considered significant (*: p<0.05; **: p<0.001; ***: p<0.0001) and indicated in the
615 figures. The specific tests used are indicated for each figure in the corresponding legend.
616